Development 138, 349-357 (2011) doi:10.1242/dev.054411

The *Drosophila Nol12* homologue *viriato* is a dMyc target that regulates nucleolar architecture and is required for dMyc-stimulated cell growth

Joana Marinho[1,2], Fernando Casares[1,3,*] and Paulo S. Pereira[1,*]

SUMMARY

The nucleolus is a subnuclear factory, the activity of which is required beyond ribosome biogenesis for the regulation of cell growth, death and proliferation. In both *Drosophila* and mammalian cells, the activity of the nucleolus is regulated by the proto-oncogene Myc. Myc induces the transcription of genes required for ribosome biogenesis and the synthesis of rRNA by RNA polymerase I, a nucleolar event that is rate limiting for cell growth. Here, we show that the fruit fly Nol12 homologue Viriato is a key determinant of nucleolar architecture that is required for tissue growth and cell survival during *Drosophila* development. We further show that *viriato* expression is controlled by *Drosophila* Myc (dMyc), and that the ability of dMyc to stimulate nucleolar and cellular growth depends on *viriato* expression. Therefore, *viriato* acts downstream of dMyc to ensure a coordinated nucleolar response to dMyc-induced growth and, thereby, normal organ development.

KEY WORDS: *Drosophila*, Cell proliferation, Cell growth, dMyc (Diminutive), Viriato, Nol12

INTRODUCTION

Tissue and organ development require a precise coordination of cellular growth, proliferation, differentiation and apoptosis. At the core of the cell, and crucial for its growth, the nucleolus is the subnuclear compartment where ribosome biogenesis takes place (Boisvert et al., 2007). Cell mass accumulation is required for proliferation, implying that the regulation of nucleolar function plays an important role in the control of proliferation rates. In the nucleolus, RNA polymerase I (Pol I) synthesizes pre-rRNAs, which are processed, modified and assembled in 40S and 60S pre-ribosomal particles that are then exported to the cytoplasm. Besides its role as the ribosome factory, the nucleolus is now also considered to be a multifunctional regulatory compartment involved in RNA processing events, sensing of cell stress, and cell cycle and apoptosis regulation (Boisvert et al., 2007).

A key step in ribosome biogenesis is pre-rRNA gene transcription by Pol I, a process that in human cells is known to be stimulated by the binding of c-MYC to rRNA promoters in the nucleolus (Arabi et al., 2005; Grandori et al., 2005). Further, *Drosophila* Myc (dMyc; also known as Diminutive – FlyBase), which is known to control the cell cycle and apoptosis, has been shown to be necessary and sufficient for the transcription of genes encoding Pol I transcription machinery factors, such as *Tif-IA* and *RpI135* (the largest Pol I subunit), genes encoding pre-rRNA processing and modifying factors, such as *Nop60B* and *Fibrillarin*, as well as a large set of ribosomal genes (Grewal et al., 2005; Pierce et al., 2008). The ability of dMyc to induce a coordinated nucleolar hypertrophy and to stimulate pre-rRNA transcription and ribosome biogenesis in general are required for dMyc-stimulated growth during *Drosophila* development (Grewal et al., 2005). Here, we identify *viriato* (*vito*) as a dMyc target gene that coordinates nucleolar and growth responses downstream of dMyc.

[1]Instituto de Biologia Molecular e Celular (IBMC), Universidade do Porto, Porto 4150-180, Portugal. [2]Ph.D. Programme in Experimental Biology and Biomedicine (PDBEB), Center for Neuroscience and Cell Biology, University of Coimbra, 3004-517 Coimbra, Portugal. [3]Centro Andaluz de Biología del Desarrollo (CABD), CSIC-JA-Universidad Pablo de Olavide. Ctra. de Utrera km1, Seville 41013, Spain.

*Authors for correspondence (fcasfer@upo.es; paulop@ibmc.up.pt)

Accepted 1 November 2010

MATERIALS AND METHODS

Fly strains and genotypes

All crosses were raised at 25°C under standard conditions. The following stocks (described in FlyBase, unless stated otherwise) were used: w^{1118}, *ptc*-Gal4, hs-Gal4, Ubi-Gal4, *ey*-Gal4, UAS-*lacZ*, UAS-bsk^{DN}, *y w* hs-flp^{122}; *act>y+>*Gal4 UAS-*GFP*, *Df(3L)H99*, y^1 w^{1118};; $p53^{[5A-1-4]}$ (*p53* null allele), *rpr*-11kb-*lacZ*, *hs*-GFP-*Nopp140True* (McCain et al., 2006), *y w hs-*flp^{122};; UAS-*dMyc*, dm^4/FM7(act-GFP), UAS-*dicer-2*, $vito^1$ [or *pBac(RB)CG32418*^{e03237}].

Eye-targeted RNAi knockdown of *vito* was induced by crossing *eyeless*-Gal4 with UAS-*vito*RNAi [Vienna Drosophila RNAi Center (VDRC) #34548]. A second UAS-*vito*RNAi transformant (named UAS-*vito*RNAiKK; VDRC #102513) was also tested and observed to generate a very similar eye phenotype. Thus, the stock UAS-*vito*RNAi (VDRC #34548) was used for most of the experiments.

Generation of UAS-*vito*, UAS-*vito*-GFP and UAS-Human*NOL12*-GFP transgenic strains

To obtain UAS-*vito* transgenic lines, the full-length *vito* cDNA was excised from the LD10447 clone (GenBank accession AY095185) as a *Not*I/*Xho*I fragment and subcloned into *Not*I/*Xho*I-digested pUAST. Transgenic lines were generated by standard germline transformation methods and five independent lines were analysed. To obtain UAS-*vito*-GFP lines, the *vito* ORF was PCR amplified from the LD10447 cDNA using Pfu polymerase (Fermentas) and primers 5′-CACCATGACCAGGAAAAAGGCT-3′ and 5′-GTCGGCATTCCGTTTGCG-3′. The amplified fragment was cloned into pENTR/D-TOPO (Invitrogen) according to the supplier's instructions. The ORF was cloned into the pUASt-GFP vector (pTWG; a gift of T. Murphy, The Carnegie Institution of Washington, Baltimore, MD, USA) by in vitro recombination using the Gateway LR Clonase II enzyme mix (Invitrogen).

UAS-Human*NOL12*-GFP flies were generated by in vitro recombination between the full ORF shuttle clone with Gateway entry vector pENTR223.1-*NOL12* (clone OCABo5050F031D, ImaGenes) and the destination vector pUASt-GFP (pTWG). The pUAS-*vito*-GFP and pUAS-

Human*NOL12*-GFP constructs were verified by DNA sequencing. Transgenic lines were generated by standard germline transformation methods and four independent lines were analysed. The Ubi-Gal4 driver was used to drive low-level expression of Vito-GFP in salivary glands, and *ey*-Gal4 was used to drive hNOL12-GFP expression during eye development and in salivary glands. *ey*-Gal4 drives 'leaky' Gal4 expression in the salivary glands.

Mitotic recombination

Mitotic recombination was induced using the Flp/FRT method. *vito* knockdown clones, or clones overexpressing dMyc alone or together with *vito*RNAi, were induced by heat shock (1 hour at 37°C) at 48 ± 4 hours after egg laying (AEL) and dissected at 118 ± 4 hours AEL in larvae of the genotype *y w hsflp*/+; act>y+>Gal4, UAS-GFP/UAS-*vito*RNAi, *y w hsflp*/+; act>y+>Gal4, UAS-GFP/+; UAS-*dMyc*/+ and *y w hsflp*/+; act>y+>Gal4, UAS-GFP/UAS-*vito*RNAi; UAS-*dMyc*/+.

Immunostaining

Eye-antennal imaginal discs were prepared for immunohistochemistry using standard protocols. Primary antibodies used were: rabbit anti-cleaved Caspase-3 at 1:200 (Cell Signaling), mouse anti-Armadillo N27A1 at 1:100 [Developmental Studies Hybridoma Bank (DSHB)], mouse anti-β-galactosidase at 1:1000 (Promega, #Z3783), rat anti-Elav 7E8A10 at 1:100 (DSHB), mouse anti-Lamin ADL101 at 1:1 (DSHB), and rabbit anti-Fibrillarin at 1:250 (Abcam, #ab5821). Appropriate Alexa Fluor-conjugated secondary antibodies were from Molecular Probes. Images were obtained with the Leica SP2 confocal system and processed with Adobe Photoshop.

In situ hybridisation

A digoxigenin (DIG)-labelled *vito* antisense RNA probe was synthesized by in vitro transcription with T7 RNA polymerase and DIG-UTP after linearisation of cDNA LD10447 with *Not*I and were used for whole-mount in situ hybridisation of fixed larvae. A sense RNA probe was used as a negative control. The DIG-labelled RNA probes were detected with an anti-DIG antibody coupled to alkaline phosphatase (Roche Diagnostics) using NBT/BCIP as substrate.

Scanning electron microscopy (SEM)

Female flies were transferred to 25% ethanol and incubated for 12-24 hours at room temperature. Flies were further dehydrated through an ethanol series (50%, 75%, and twice 100%; 12-24 hours each step) before being incubated twice for 30 minutes each with hexamethyldisilazane, air-dried overnight, mounted onto SEM stubs covered with carbon tape, and sputter coated with platinum. Samples were imaged using an FEI Quanta 400 microscope.

Transmission electron microscopy (TEM)

Dissected third instar salivary glands were fixed with 2.5% glutaraldehyde in 0.1 M sodium cacodylate buffer for 30 minutes and post-fixed with 4% osmium tetroxide. After washing, salivary glands were incubated with 0.5% uranyl acetate (30 minutes) and further dehydrated through a graded ethanol series (70% for 10 minutes, 90% for 10 minutes, and four changes of 100%). Salivary glands were then soaked in propylene oxide for 10 minutes and then in a mixture (1:1) of propylene oxide and Epon resin (TAAB Laboratories) for 30 minutes. This mixture was then replaced by 100% Epon resin for 24 hours. Finally, fresh Epon replaced the Epon and polymerisation took place at 60°C for 48 hours. Ultrathin sections were obtained using an ultramicrotome, collected in copper grids and then double contrasted with uranyl acetate and lead citrate. Micrographs were taken using a Zeiss EM10C electron microscope (80 kV).

Quantitative real-time PCR (qPCR)

For the experiment in which *vito*RNAi was ubiquitously induced, RNA was isolated from control (Ubi-Gal4/+) or *vito*RNAi (Ubi-Gal4/+; UAS-*vito*RNAi/+) larvae 112 hours AEL. RNA was also isolated from control (*w1118*) and *vito*^{1} homozygous wandering third instar larvae. Ubiquitous dMyc overexpression in wandering third instar larvae was induced by giving a heat shock (1 hour at 37°C) to hs-Gal4/UAS-*dMyc* larvae that were collected 4 hours after the heat shock. Control hs-Gal4/+ larvae were subjected to the same treatment.

For dMyc loss-of-function experiments, total RNA was isolated from either *dm*^{4} mutant or control larvae 24 hours AEL. Total RNA was also isolated from third instar salivary glands of the genotypes control (UAS-*lacZ*/+; *ptc*-Gal4/+), dMyc^{OE} (*ptc*-Gal4/+; UAS-*dMyc*/+), dMyc^{OE}+*vito*RNAi (*ptc*>Gal4/UAS-*vito*RNAi; UAS-*dMyc*/+) and from eye imaginal discs of genotypes control (*ey*-Gal4/+) and *vito*RNAi (*ey*-Gal4/UAS-*vito*RNAi). Total RNA was isolated using TRIzol (Invitrogen) according to the manufacturer's instructions and treated with DNase I (RNase-free; Ambion). cDNA was generated by reverse transcription with the SuperScript III First-Strand Synthesis SuperMix for qRT-PCR (Invitrogen). Quantitative real-time PCR analysis was performed in triplicate in 20 μl reactions containing iQ SYBR Green Supermix (BioRad), each gene-specific primer at 250 nM and 1 μl of cDNA template. Cycling conditions in a BioRad iQ5 instrument were 95°C for 3 minutes, followed by 40 cycles of denaturation at 95°C for 10 seconds and annealing for 30 seconds at 60 or 64°C depending on the primer set. Fold change relative to the expression of *CaMKII*, which has been used previously as a control for gene expression in *dm*^{4} mutants and for overexpression of *dMyc* in the whole larvae (Pierce et al., 2004), was calculated using the $2^{-\Delta\Delta CT}$ method (Livak and Schmittgen, 2001). For salivary glands, data were normalised for levels of total RNA. Three to five biological replicates were analysed for each primer set. Values are presented in $\log_2$ scale or as absolute expression levels. Statistical significance was determined using the Relative Expression Software Tool [REST; http://rest.gene-quantification.info (Pfaffl et al., 2002)]. The mathematical model is based on randomisation tests, which have the advantage of making no distributional assumptions about the data.

The following primer pairs (5′ to 3′) were used:

CaMKII (control), TTACACCATCCCAACATAGTGC and CAAGGTCAAAAACAAGGTAGTGATAG;

Nop60B, GAGTGGCTGACCGGTTATGT and GCTGGAGGTGCTTAACTTGC;

p53, GCGAAAAGAAACTTCCTTAGTCTTC and TTGGGGCACGTACATATTTTAAC;

Tif-IA, CAAGCCTATTTTCGAAGAACTTGT and CAAGGTGTCCGCTTCCAC;

Rpl135, CCCGGAGTTTAAGCAGATACC and CACATGTGGACCTCCCAAA;

*vito*qPCR1 (to detect *vito* transcript levels in *vito*RNAi experiments), GACCAGGAAAAAGGCTCCTAA and TTGCGCTCGTTCTTAAGGTT;

*vito*qPCR2 (to detect *vito* transcript levels in *vito*^{1} homozygous larvae), AGGTGAAGATCGTGGAGCTGAC and CCTGGTCGGCTTCGTCCTC;

Fibrillarin (*Fib*), GCATCTCCGTTGAGACCAAT and GACACATGCGAGACTGTCGT;

pre-rRNA (ETS), GCTCCGCGGATAATAGGAAT and ATATTTGCCTGCCACCAAAA;

rpr, CATACCCGATCAGGCGACTC and CGGATGACATGAAGTGTACTGG; and

puc, AGGCTATGGACGAGGATGGGTTTG and GGCGGCGAGGTCAATCTGGATG.

Size and volume measurements and statistics

Eye disc areas were measured using the Straight Line tool of ImageJ 1.41o software (NIH, Bethesda, MA, USA), considering only the eye disc from the eye-antennal imaginal disc. In all the disc-proper clones assessed for clone size, nuclei were counted in the DAPI channel. Cell size estimates were obtained by dividing each clone area by the number of nuclei in the clone. For the comparison of nuclear, cytoplasmic and cell sizes in different genetic backgrounds, the radius (r) was measured using the Straight Line tool of ImageJ. Volume (V) was approximated as $V=4/3\ \pi\ r^3$. For each genotype, 62-82 nuclei were scored. GraphPad Prism 5.0 was used for statistical analysis and for generating the graphical output. Statistical significance was determined using an unpaired two-tailed Student's *t*-test, with a 95% confidence interval, after assessing the normality distribution of the data with the D'Agostino-Pearson normality test.

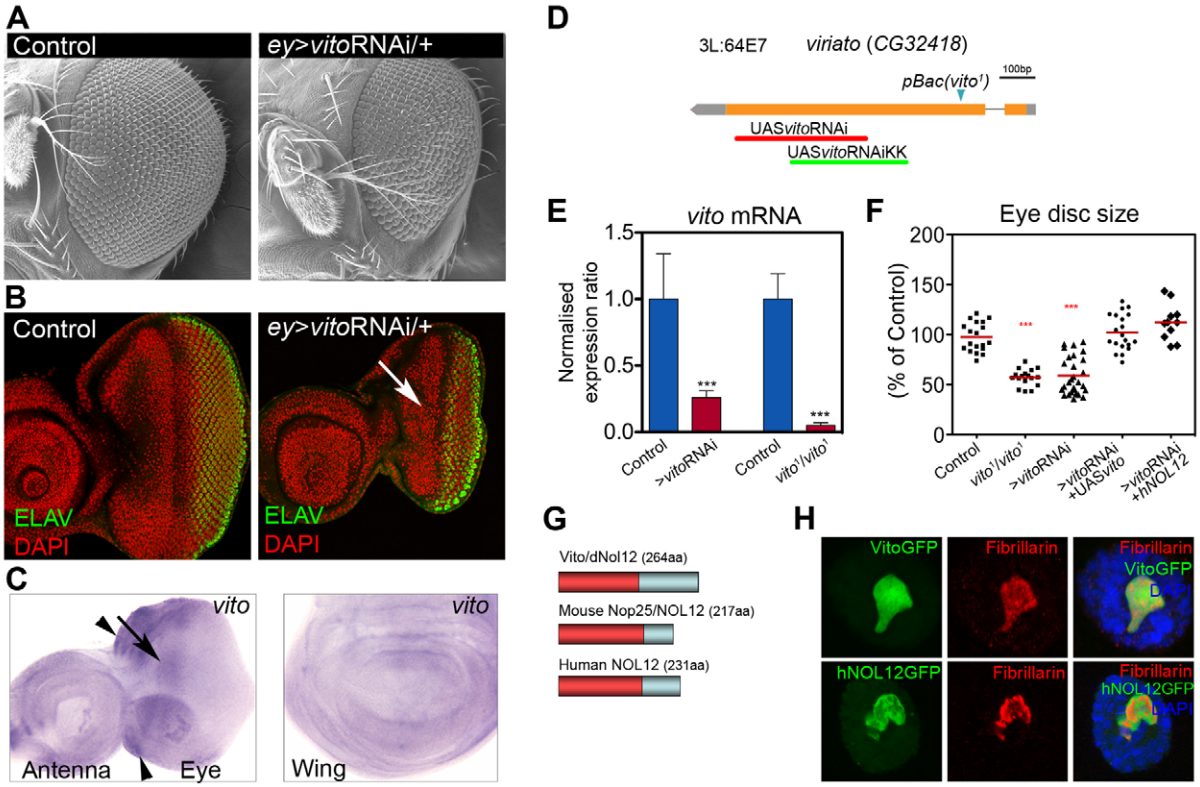

Fig. 1. *vito* encodes a nucleolar protein required for tissue growth. (**A**) Lateral views of control (*ey*-Gal4/+) and *vito* loss-of-function (*ey*>*vito*RNAi/+ is *ey*-Gal4, UAS-*vito*RNAi/+) adult *Drosophila* eyes. (**B**) Depleting *vito* in the eye causes a decrease in the size of eye primordia (arrow). Eye discs were stained with a photoreceptor-specific antibody (anti-Elav, green) and with DAPI for DNA (red). (**C**) RNA in situ hybridisation shows that *vito* is widely expressed in imaginal discs. In the eye disc, expression is higher in the anterior proliferating region of the disc (arrow). The dorsal and ventral margin regions show a non-specific signal (arrowheads; see also Fig. S2 in the supplementary material). (**D**) The *CG32418*/*vito* genomic region. Boxed regions represent the two *vito* exons and orange indicates the coding region. The two distinct regions targeted by the independent *vito*RNAi lines used are indicated beneath, and the position of the *PiggyBac* insertion in exon 2 of the $vito^1$ mutant allele ($PBac\{RB\}CG32418^{e03237}$) is indicated above. (**E**) *vito* mRNA levels were measured by qPCR using RNA isolated from control larvae or those ubiquitously expressing *vito*RNAi at 112 hours after egg laying (AEL), and from $vito^1$ homozygous larvae and wild-type controls. Data are presented as fold change relative to control and indicate the mean + s.d. (n=3-5). Data were normalised to the levels of *CaMKII* mRNA. ***, $P<1\times10^{-4}$ relative to control). (**F**) Eye disc sizes of the indicated genotypes represented as a distribution. Dots represent individual measurements and horizontal bars show mean values (***, $P<1\times10^{-4}$ relative to control). Control (UAS-*lacZ*/+; *ey*-Gal4/+); >*vito*RNAi (*ey*-Gal4, UAS-*vito*RNAi/+); >*vito*RNAi + UAS*vito* (UAS*vito*/+; *ey*-Gal4, UAS-*vito*RNAi/+); *vito*RNAi + h*NOL12* (*ey*-Gal4, UAS-*vito*RNAi/+; UASh*NOL12*-GFP/+). (**G**) Domain structure of Vito and human and mouse NOL12 homologues. The N-terminus of Vito is 28% identical to the N-terminus of human NOL12. (**H**) Nucleolar localisation of Vito-GFP and human NOL12-GFP in *Drosophila* larval salivary gland cells co-stained for the nucleolar protein Fibrillarin (red) and with DAPI for DNA.

RESULTS

vito encodes the single *Drosophila* member of the conserved Nol12 family of nucleolar proteins and is required for tissue growth

In a search to identify genes required for tissue growth in *Drosophila*, we observed that expression of an RNAi transgene targeting the uncharacterised *CG32418* gene [which we named *viriato* (*vito*)] in the developing eye resulted in a reduced and rough eye (Fig. 1A and see Fig. S1 in the supplementary material). When we examined the effects of *vito*RNAi expression in the eye primordium, we observed that although posterior retinal differentiation still occurred, a very significant reduction in eye disc size was visible, particularly in the anterior proliferative region of the disc (Fig. 1B and see Fig. S1 in the supplementary material). This suggested that *vito* is required for growth and/or proliferation before the onset of photoreceptor differentiation. In support of this hypothesis, although widely transcribed in imaginal discs, *vito* expression is stronger in the anterior region of the eye disc (Fig. 1C and see Fig. S2 in the supplementary material). Similar phenotypes in eye discs and adults were observed with a second RNAi line (UAS-*vito*RNAiKK) and in eye discs homozygous for the $vito^1$ allele ($vito^1$ results from a *PiggyBac* insertion, $PBac\{RB\}CG32418^{e03237}$) (Fig. 1 and see Fig. S1 in the supplementary material). In addition, reduction of *vito* levels, either in $vito^1$ homozygous larvae or induced by generalised expression of *vito*RNAi, caused a significant developmental delay (see Fig. S3 in the supplementary material). Very significant reductions of *vito* mRNA levels were detected by qPCR in larvae expressing *vito*RNAi and in $vito^1$ homozygous larvae (Fig. 1E). To confirm the specificity of the phenotypes observed, we attempted to rescue the effects of *vito*RNAi by co-expressing a full-length *vito* cDNA. Indeed, eye disc size (Fig. 1F and see Fig. S1 in the supplementary material), adult eye size and morphology and several other cellular parameters (see below, and see Fig. S1 in the supplementary material) were significantly rescued by supplying *vito* back.

Sequence comparison analysis predicts *vito* to encode a small protein with an N-terminal Nol12 domain that is conserved in the Nol12 protein family (Fig. 1G). The *Drosophila* genome contains only one non-redundant gene for Nol12, as do all the genomes found to encode Nol12 proteins. Therefore, we attempted to rescue the reduced growth induced by *vito*RNAi by co-expressing the single human NOL12 (hNOL12) protein. Remarkably, hNOL12 was also able to fully rescue eye disc growth, suggesting that there is an evolutionary conservation of Nol12 protein family functions in tissue growth (Fig. 1F and see Fig. S1 in the supplementary material). We concluded from these results that inducible *vito*RNAi was efficient and specific, which, together with the ease and flexibility of *vito* knockdown in both clones and targeted tissues, led us to mainly use *vito*RNAi for the experiments described here.

Human NOL12 has been identified in several proteomic analyses of human nucleoli (Ahmad et al., 2008). Mouse NOL12 localises to nucleoli in COS7 cells, and knocking down NOL12 function in this cell line results in nucleolar fragmentation (Suzuki et al., 2007). In budding yeast, the Nol12 homologue Rrp17p/Ydr412p has been implicated in nucleolar non-coding RNA processing events (Peng et al., 2003; Li et al., 2009; Oeffinger et al., 2009). Owing to the relatively low conservation of the Nol12 domain, we analysed whether Vito localised to the nucleolus. Targeted expression of low levels of GFP-tagged Vito in *Drosophila* tissues showed colocalisation of Vito with Fibrillarin (Fig. 1H; and also in S2 cells, see Fig. S4 in the supplementary material), a nucleolar methyltransferase required for pre-rRNA modification that localises to the fibrillar region of *Drosophila* nucleoli (Orihara-Ono et al., 2005). Consistent with its ability to functionally compensate for *vito* knockdown, hNOL12 also localised to the nucleolus when expressed in *Drosophila* larval tissues (Fig. 1H).

Since no in vivo functional information is thus far available for members of the Nol12 family in any metazoan, we examined the role of *vito* in tissue growth during *Drosophila* development. Using Flp/FRT-based recombination, we induced during early larval development clones of cells expressing *vito*RNAi that were analysed later in third instar eye imaginal discs. During this period, most cells in the disc are actively proliferating. In the eye disc, *vito*RNAi-expressing clones were significantly smaller than control neutral clones, both in the peripodial epithelium and in the eye disc proper (Fig. 2A-C). This was not due to a reduction in cell size (Fig. 2D and see Fig. S5 in the supplementary material), suggesting that in proliferating cells *vito* knockdown slows down proliferation while maintaining the coordination of cell growth and cell cycle.

vito is required for tissue growth independently of its role in cell survival

Next, we investigated whether *vito* misregulation could also result in apoptosis, contributing to the observed defect in tissue growth. In contrast to wild-type eye discs, where apoptosis is virtually absent during larval development, *vito*RNAi eye discs exhibited a significant number of cells undergoing apoptosis, as detected by the presence of activated cleaved Caspase-3 (Decay – FlyBase) (Fig. 3A,B), and this was accompanied by a substantial reduction in disc size (42%, $P<1\times10^{-4}$; Fig. 3C). Therefore, *vito* is required for cell survival.

To determine whether the reduction in disc size could be explained exclusively by this increase in apoptosis, *vito*RNAi was induced in a heterozygous background for the *H99* deficiency (Fig. 3A), which deletes the three crucial proapoptotic genes

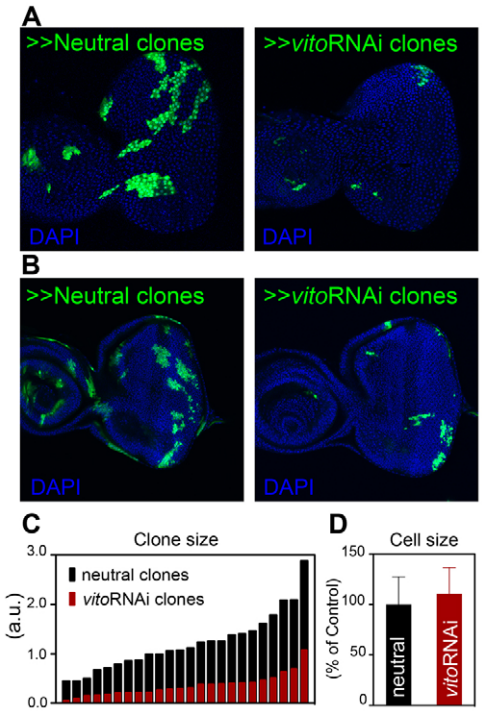

Fig. 2. *vito*RNAi clones have a growth disadvantage. (**A**,**B**) Neutral or *vito*RNAi clones were induced in the *Drosophila* early eye disc and analysed 72 hours later. Images show representative clones in the peripodial epithelium (A) and epithelial layers of the disc proper (B), marked positively by the presence of GFP. (**C**) Quantification of neutral and *vito*RNAi clone size in the eye disc proper represented as clonal area distributions. (**D**) Mean cell size (+ s.d.) in eye disc-proper clones obtained by dividing each clonal area by the number of nuclei in the clone (n=24). a.u., arbitrary units.

reaper (*rpr*), *grim* and *hid* (*Wrinkled* – FlyBase) (White et al., 1994; Grether et al., 1995; Chen et al., 1996). In this genotype, in which apoptosis was almost completely suppressed (Fig. 3B), the average size of the eye disc was only partly rescued compared with *vito*RNAi discs (22%, P=0.0072), but was still significantly smaller than in control discs (29% reduction, $P<1\times10^{-4}$) (Fig. 3C). Similar results were obtained when *vito*RNAi was co-induced with the baculovirus caspase inhibitor p35 (see Fig. S6 in the supplementary material). Furthermore, even though we only detected a slight, non-statistically significant increase in *rpr* transcript levels by qPCR in whole eye-antennal *vito*RNAi discs (Fig. 3D), we observed a robust and localised upregulation of the *rpr*-11kb-*lacZ* transcriptional reporter (Nordstrom et al., 1996) in the anterior proliferative domain of the eye disc (Fig. 3E). Interestingly, most of the apoptotic death was detected in the anterior domain, where we had also detected the strongest *vito* transcription. The fact that only a fraction of cells within the eye disc upregulated *rpr* (as monitored by the *rpr*-11kb-*lacZ* reporter) might have masked the increase in *rpr* transcripts in whole discs measured by qPCR.

Overall, these results indicate that the growth deficit induced by reducing *vito* function cannot be explained by a generalised induction of apoptosis. Since Vito is a nucleolar protein and nucleolar stress in mammalian cells leads to apoptosis mediated by p53 stabilisation (Rubbi and Milner, 2003; Yuan et al., 2005), we tested whether apoptosis in *vito*RNAi eye cells was

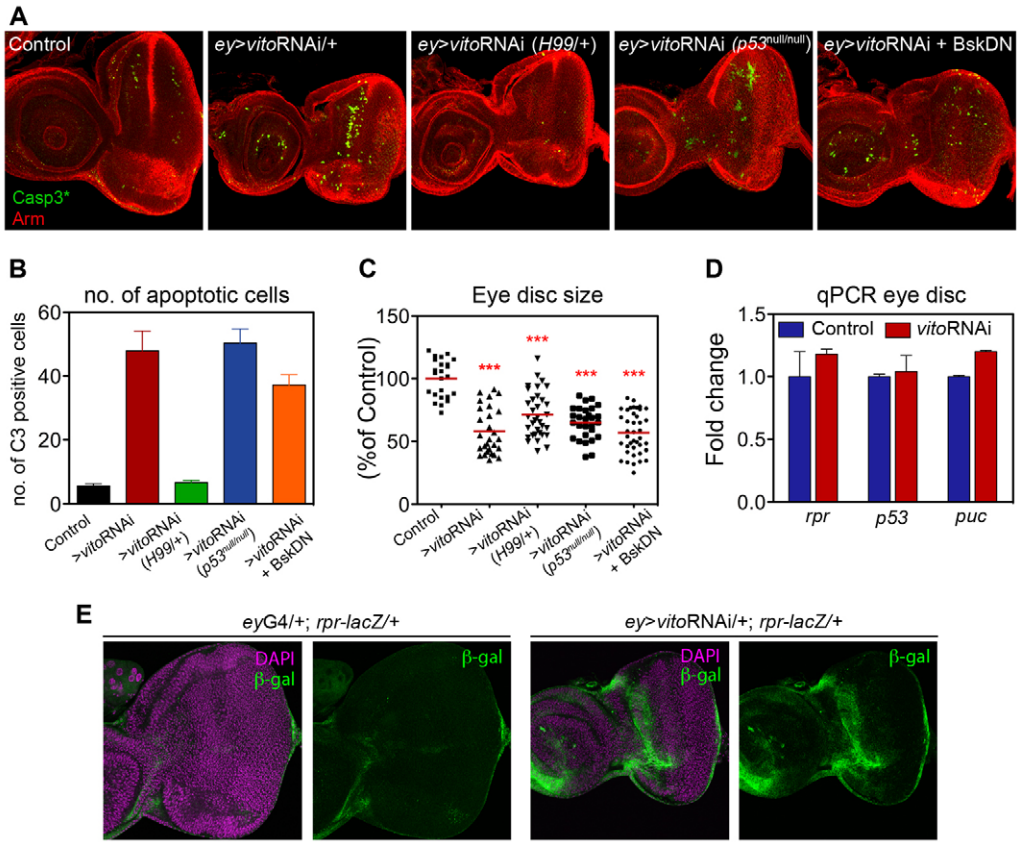

Fig. 3. *vito* is required for tissue growth independently of its role in cell survival. (**A**) Late third instar *Drosophila* eye imaginal discs of the indicated genotypes stained for Armadillo (red) and cleaved Caspase-3 (green). Knocking down *vito* (*ey>vito*RNAi) affects the size of the eye discs and causes significant cell death. Removing one copy of each of the three pro-apoptotic genes of the Hid-Reaper-Grim complex by introducing the deficiency *H99* into the *vito*RNAi background (*ey>vito*RNAi/+; *H99*/+) blocks cell death in the eye imaginal disc. *vito*RNAi tissue growth and cell death phenotypes are not rescued in *p53* null mutant eye discs (*ey>vito*RNAi/+; p53*null*). Overexpression of a dominant-negative form of JNK (BskDN) in the *vito*RNAi background (*ey>vito*RNAi/+; UASBsk^{DN}) does not rescue the tissue growth phenotype. Control (UAS-*lacZ*/+; *ey*-Gal4/+); >*vito*RNAi (*ey*-Gal4, UAS-*vito*RNAi/+); >*vito*RNAi (*H99*/+) (*ey*-Gal4, UAS-*vito*RNAi/+; *Df(3L)H99*/+); >*vito*RNAi (*p53*$^{null/null}$) (*ey*-Gal4, UAS-*vito*RNAi/+; *p53*$^{[5A\text{-}1\text{-}4]}$/*p53*$^{[5A\text{-}1\text{-}4]}$); >*vito*RNAi + BskDN (*ey*-Gal4, UAS-*vito*RNAi/+; UASBsk^{DN}/+). (**B**) Quantification of cell death assessed by the number of cleaved Caspase-3-positive cells in the eye discs in A. The significant number of cells undergoing apoptosis in *vito*RNAi eye discs is abolished in a heterozygous background for the *H99* deficiency. Data are presented as the mean + s.e.m. (n=15-40). (**C**) Eye disc sizes of the indicated genotypes were measured and are represented as a distribution. Dots represent individual measurements and horizontal bars show mean values (***, $P<1\times10^{-4}$ relative to control). (**D**) Transcript levels of genes involved in the apoptotic pathway were measured by qPCR using RNA isolated from either control or *vito*RNAi eye imaginal discs. Data are presented as the fold change compared with the control and represent the mean + s.d. (n=3). (**E**) The expression of *reaper* (*rpr*) was monitored using the *rpr*-11kb-*lacZ* reporter in control and *vito*RNAi eye discs. Eye discs were stained with an anti-β-galactosidase antibody (green) and with DAPI for DNA (purple). Increased levels of *rpr* reporter activity are detected in the anterior region of *vito*RNAi eye discs.

dependent on p53 function. Expression of *vito*RNAi still caused a significant level of apoptosis in a *p53* null mutant background (Fig. 3A,B), or when co-expressed together with a dominant-negative form of p53 (R155H) (see Fig. S6 in the supplementary material) that is able to block p53 pro-apoptotic activity (Ollmann et al., 2000). The absence of p53 function did not rescue normal tissue growth in *vito*RNAi eye discs (Fig. 3C). In addition, we could not detect elevated p53 transcript or protein levels in *vito*RNAi eye discs (Fig. 3D and see Fig. S6 in the supplementary material).

In *Drosophila*, as well as in mammals, the c-Jun N-terminal kinase (JNK) pathway has been implicated in apoptotic cell death in a variety of cellular and developmental contexts (reviewed by Igaki, 2009), and has been suggested to act both upstream (McEwen and Peifer, 2005) and downstream (Kuranaga et al., 2002) of *rpr* function. We studied the possible involvement of JNK signalling in apoptosis resulting from *vito*RNAi expression by: (1) co-expressing a dominant-negative form of JNK (BskDN) (Fig. 3A); and (2) analysing *puc* transcript levels (Fig. 3D) and *puc-lacZ* reporter transcription (see Fig. S6 in the supplementary material) as a read-out for JNK signalling (Martin-Blanco et al., 1998). The results of these experiments suggest that upon *vito* knockdown there is a weak activation of JNK signalling, as *puc* mRNA levels in eye discs increased by 20% (but in a non-significant manner, P=0.059) (Fig. 3D), and the co-expression of BskDN resulted in minor apoptotic rescue (Fig. 3A,B). We also failed to detect any upregulation of *puc-lacZ* in *vito*RNAi clones in eye discs (see Fig. S6 in the supplementary material), suggesting that activation of JNK signalling is not the major pathway that mediates the apoptotic process resulting from *vito* knockdown.

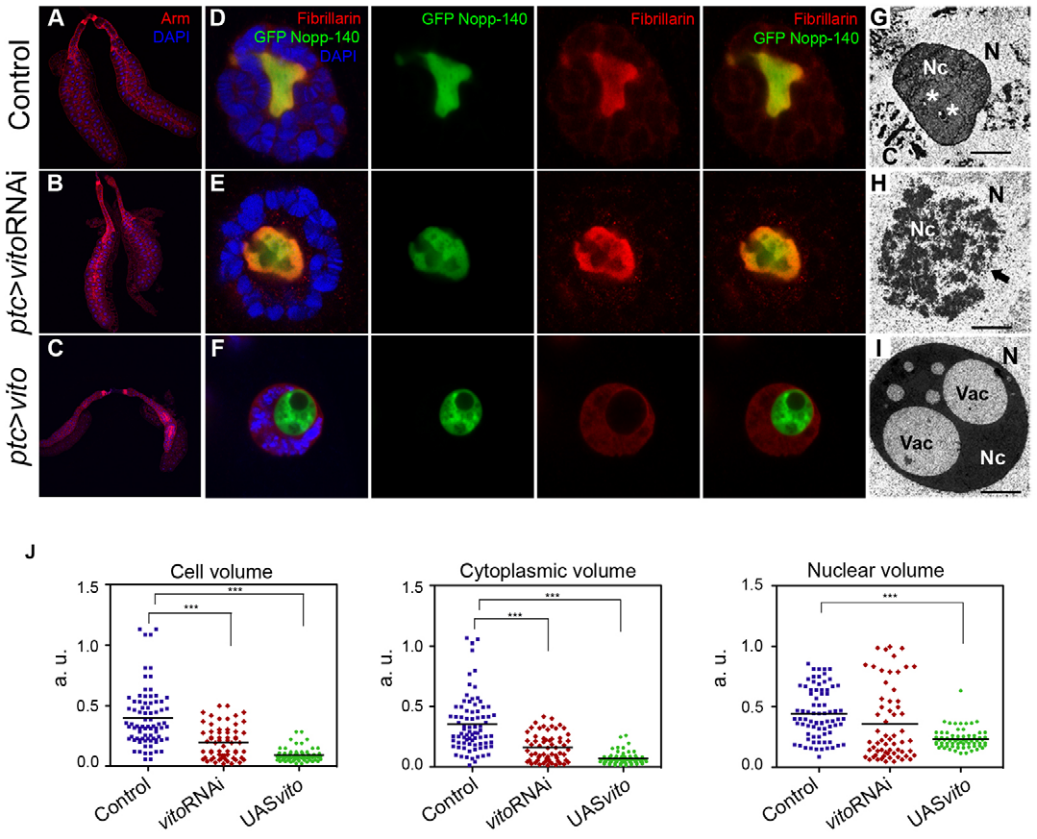

Fig. 4. Vito regulates nucleolar structure. (**A-I**) Salivary glands show a substantial reduction in overall size upon *vito* misregulation. Low magnifications of salivary glands from third instar *Drosophila* larvae expressing UAS-*lacZ* (control) (A,D,G), UAS-*vito*RNAi (B,E,H) and UAS-*vito* (C,F,I) under the control of the *ptc-Gal4* driver. (D-F) Vito regulates nucleolar localisation of Fibrillarin. Third instar larvae heterozygous for the insertion hs-GFP-Nopp140-True were heat shocked for 1 hour and allowed to recover for 2 hours. (D) GFP-Nopp140-True (green) and Fibrillarin (red) colocalise in the nucleolus of control salivary gland cells. (E) Fibrillarin accumulates preferentially in the nucleolar periphery of *vito*RNAi-expressing cells. (F) Vito-overexpressing cells show a swollen and abnormally rounded nucleolus that loses Fibrillarin staining. (G-I) Reducing Vito levels results in nucleolar decondensation, whereas overexpressing Vito causes the opposite phenotype, with the nucleolus becoming a very dense and compact structure. (G-I) Electron micrographs of control salivary glands (G), *vito*RNAi (H) or salivary glands overexpressing Vito (I). Asterisks indicate small vacuoles and Vac indicates large vacuolar-like regions. The arrow indicates granular regions. N, nucleus; Nc, nucleolus. Scale bars: 2 μm. (**J**) Scatter plots showing cellular, cytoplasmic and nuclear volumes in salivary glands of the indicated genotypes (n=62-80; ***, $P<1\times10^{-4}$).

Overall, these experiments show that *vito* is required for tissue growth during *Drosophila* development. This requirement can be explained only in part by the role of *vito* in preventing caspase-mediated apoptosis, in which the JNK pathway itself might play a marginal role.

vito regulates nucleolar structure and nucleolar retention of Fibrillarin

To investigate further the mechanisms by which Vito, a nucleolar protein, might be controlling tissue growth, we analysed the effects of reducing or increasing Vito levels on the nucleolus of salivary gland cells, which, owing to their polyploidy, have large nucleoli. As in the eye disc, the reduction of *vito* expression in the salivary glands also caused a substantial deficit in tissue growth (Fig. 4A,B). To examine nucleolar structure and activity we looked at the distribution of Fibrillarin and *Drosophila* Nopp140-True (Cui and DiMario, 2007). The human NOPP140 (NOLC1) protein is a conserved phosphoprotein that interacts with the RNA Pol I 194 kDa subunit (RPA194) and is proposed to play a role in the maintenance of nucleolar structure (Chen et al., 1999). NOPP140 is also required for the assembly or recruitment of small nucleolar ribonucleoproteins (snoRNPs) to the nucleolus, where these complexes guide site-specific 2′-O-methylation and pseudouridylation of pre-rRNA (Wang et al., 2002). In *Drosophila*, as previously described (McCain et al., 2006), a GFP-tagged Nopp140-True protein expressed from a heat shock-inducible promoter was detected uniformly in the nucleolus of salivary gland cells, where it colocalised with Fibrillarin (Fig. 4D). In *vito*RNAi-expressing cells, Nopp140-True still localised to the nucleolus but its pattern became more dispersed and ‘hollow’, concentrating at the nucleolar periphery. This redistribution paralleled the redistribution of Fibrillarin, which was concentrated in the nucleolus at significantly higher levels (Fig. 4E; for similar results with $vito^{1}$ mutants and rescue with Vito and hNOL12, see Fig. S7 in the supplementary material). In *vito*-overexpressing cells (Fig. 4C), Nopp140-True was still recruited to the nucleolus, which became rounded and displayed large vacuoles devoid of Nopp140 signal. Interestingly, Fibrillarin was absent from Vito-overexpressing nucleoli and accumulated at low levels in the nucleoplasm (Fig. 4F, and see Fig. S4 in the supplementary material for similar results in S2 cells).

These changes in nucleolar morphology resulting from altering Vito expression levels were confirmed by TEM (Fig. 4G-I). As previously noted (Orihara-Ono et al., 2005), the wild-type *Drosophila* nucleolus does not display the characteristic vertebrate tripartite organisation, as only a homogeneous region with a regular surface is observed (Fig. 4G). Knocking down *vito* resulted in a substantial reduction in the packaging of nucleolar components, and the nucleoli exhibited a clear overall granular organisation (Fig. 4H). By contrast, Vito overexpression induced a dramatic re-organisation of the nucleolus into two distinct regions: a peripheral and highly compact region with very smooth borders that surrounded internal vacuole-like structures (Fig. 4I).

These results show that Vito is a major regulator of nucleolar architecture and that it regulates the recruitment of specific nucleolar components: whereas Nopp140 remains associated to the nucleolus when Vito levels are changed, the recruitment of the snoRNP methyltransferase Fibrillarin depends critically on Vito. Interestingly, in human cells, NOPP140, but not fibrillarin or the rRNA pseudo-uridylase dyskerin, can interact with ribosomal gene chromatin independently of ongoing Pol I transcription (Prieto and McStay, 2007). This suggests that Vito could act to control the recruitment or retention of a second layer of proteins, such as Fibrillarin, that require binding to nucleolar hub proteins (Emmott and Hiscox, 2009) in order to associate with the nucleolar compartment.

Vito levels modulate mass accumulation

We next aimed to establish correlations between the observed nucleolar alterations and tissue growth deficit caused by *vito* misregulation in salivary gland cells. Firstly, quantification of estimated salivary gland cell volumes revealed that both *vito*RNAi and Vito-overexpressing gland cells were significantly smaller than controls (51% and 77% reductions, respectively; $P<1\times10^{-4}$; Fig. 4J). However, we noted significant differences in the impact of increasing or decreasing *vito* on cytoplasmic and nuclear sizes. The size reduction in *vito*RNAi-expressing cells was basically due to a reduction in cytoplasmic volume (55%, $P<1\times10^{-4}$), as nuclear volumes were not significantly reduced (20%, $P=0.0228$). This suggests that *vito* knockdown mainly affects cytoplasmic mass accumulation, while not interfering with the endoreplication process, something that we also assessed by quantifying DAPI staining intensity (see Fig. S7 in the supplementary material). Vito overexpression caused not only a substantial reduction in cytoplasmic volume (81% $P<1\times10^{-4}$), but also a decrease in nuclear size (48%, $P<1\times10^{-4}$). However, this nuclear size reduction might be secondary to the dramatic loss of cytoplasmic mass: it is likely that the extremely aberrant nucleolar morphology compromises basic cellular processes such as protein synthesis, indirectly affecting DNA endoreplication (and hence nuclear size), as these two processes are intimately linked (reviewed by Edgar and Orr-Weaver, 2001).

vito is a dMyc target required for dMyc-stimulated growth

Our results showing that *vito* is required for the proliferation of diploid imaginal cells and for the growth of polyploid salivary gland cells led us to hypothesize that *vito* could act downstream of dMyc, a crucial regulator of *Drosophila* growth (Johnston et al., 1999) that is also known to be a major regulator of nucleolar growth (Grewal et al., 2005). Since dMyc stimulates tissue growth in part by activating the transcription of genes required for nucleolar function and ribosome biogenesis (Grewal et al., 2005; Demontis and Perrimon, 2009), we tested whether *vito* transcription was under dMyc control. Indeed, dMyc strongly regulated *vito* mRNA levels (Fig. 5). When quantified by qPCR, *vito* transcript levels were reduced by 85% in larvae homozygous for the null $dMyc^{dm4}$ allele, and increased 1.9-fold and 18.9-fold upon dMyc overexpression in whole larvae and in salivary glands, respectively (Fig. 5A).

We next assessed whether *vito*RNAi affected the transcriptional response of several known dMyc targets (Grewal et al., 2005; Pierce et al., 2008). The set of targets analysed included genes encoding factors involved in pre-rRNA transcription (the Pol I subunit *RpI135* and the basal Pol I *Tif-IA* transcription factor), genes encoding pre-rRNA processing/modifying enzymes [the pseudo-uridylase *Nop60B* (the *Drosophila* homologue of dyskerin) and *Fibrillarin*] and also primary pre-rRNA transcripts [containing the external transcribed spacer (ETS) region]. As expected, dMyc

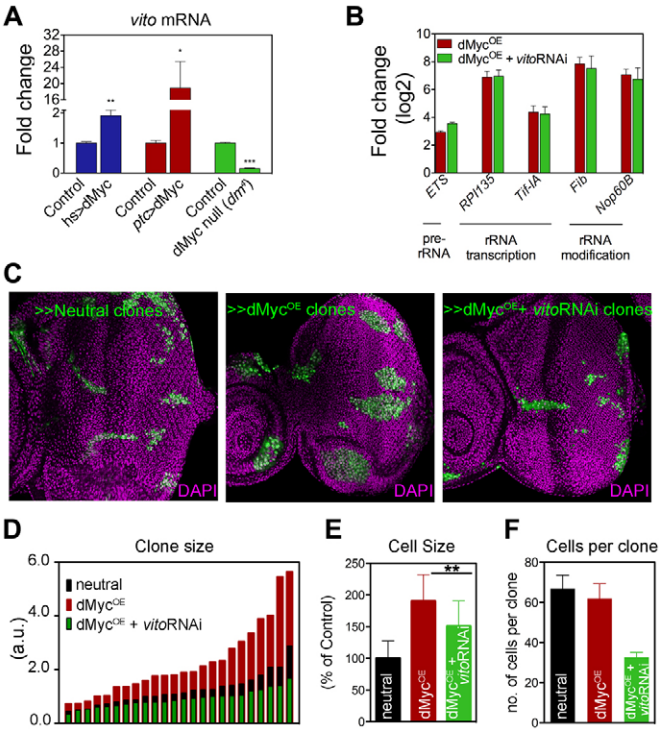

Fig. 5. *vito* is a dMyc transcriptional target required for dMyc-stimulated growth. (**A**) *vito* mRNA levels were measured by qPCR upon heat shock-induced expression of dMyc in *Drosophila* third instar larvae, in salivary glands of third instar larvae overexpressing *dMyc* from the *ptc*-Gal4 driver, and in *dMyc* null (dm^4 allele) first instar larvae. *, $P<0.01$; **, $P<0.001$; ***, $P<1\times10^{-4}$ relative to control. (**B**) Transcript levels of genes involved in rRNA transcription and modification were measured by qPCR using RNA isolated from salivary glands of third instar larvae of the indicated genotypes. In A and B, data are presented as fold changes ($\log_2$) compared with the control and represent the mean + s.d. (n=3-5). Control (UAS-*lacZ*/+; *ptc*-Gal4/+), $dMyc^{OE}$ (*ptc*-Gal4/+; UAS-*dMyc*/+), $dMyc^{OE}$ + *vito*RNAi (*ptc*>Gal4/UAS-*vito*RNAi; UAS-*dMyc*/+). (**C**) dMyc-expressing clones ($dMyc^{OE}$) in the eye disc are larger than control clones. Co-expression with *vito*RNAi reduces dMyc-stimulated clone growth. Clones were marked positively by the presence of GFP, which was induced in the eye disc at 48 ± 4 hours AEL, and analysed at 118 ± 4 hours AEL. (**D**) Clonal size distribution of the above genotypes in the eye disc proper (n=24). (**E**) The average cell size (+ s.d.) within the clones (n=24). **, P=0.0012. (**F**) The number of cells of each clone was also scored and is represented as the mean + s.e.m. (n=24).

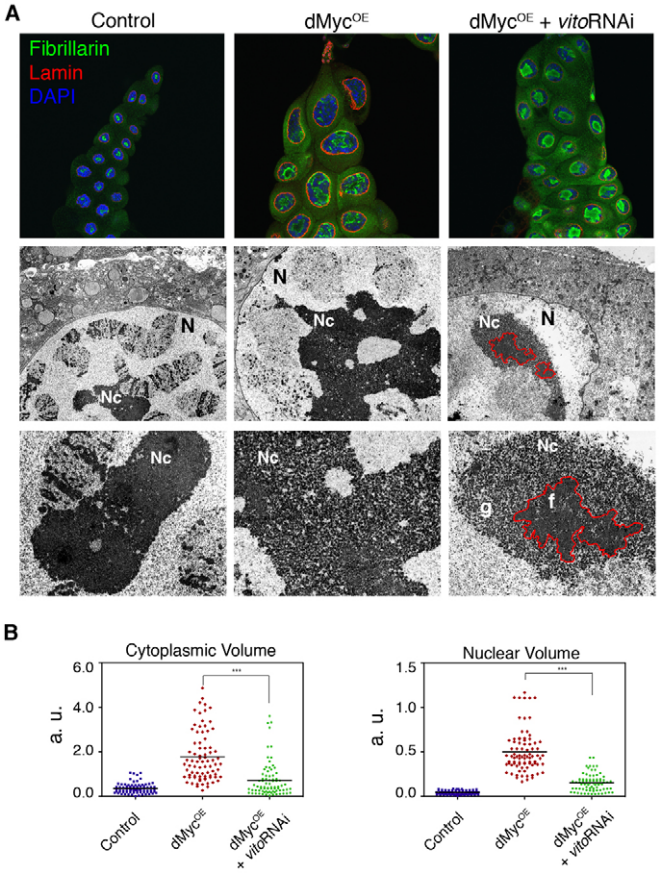

Fig. 6. *vito* is required for nucleolar integrity during dMyc-stimulated growth. (**A**) In *Drosophila* salivary gland cells, the substantial increases in cytoplasmic and nuclear volumes induced by dMyc^{OE} are significantly attenuated by *vito*RNAi co-expression. Salivary glands of the indicated genotypes were stained for the nucleolar marker Fibrillarin (green), Lamin B to reveal the nuclear envelope (red), and counterstained with DAPI (blue) (top row). Shown are transmission electron micrographs of nuclear regions of salivary gland cells (middle row) and corresponding magnifications of the nucleoli (bottom row). The red line highlights the fibrillar region that segregates from a granular component in dMyc^{OE}+*vito*RNAi nucleoli. N, nucleus; Nc, nucleolus; f, fibrillar; g, granular. (**B**) Quantification of nuclear and cytoplasmic volumes after overexpressing dMyc alone or together with UAS-*vito*RNAi (n=80-82). ***, $P<1\times10^{-4}$. Control (UAS-*lacZ*/+; *ptc*-Gal4/+), dMyc^{OE} (*ptc*-Gal4/+; UAS-*dMyc*/+), dMyc^{OE} + *vito*RNAi (*ptc*>Gal4/UAS-*vito*RNAi; UAS-*dMyc*/+).

overexpression induced strong upregulation of all these target transcripts in salivary glands. However, co-expression of *vito*RNAi did not affect their strong induction by dMyc (Fig. 5B). Therefore, *vito* does not appear to be required for the transcriptional induction of dMyc target genes involved in nucleolar growth and ribosome biogenesis.

To test whether *vito* function is required for dMyc-stimulated growth, we overexpressed dMyc in the diploid proliferative eye disc cells, in the presence and absence of *vito*RNAi. Whereas mitotic clones expressing dMyc were significantly larger than control clones, the co-expression of dMyc with *vito*RNAi resulted in a reduction in clone size relative to control levels (Fig. 5C,D). This reduction was the consequence of a partial reversion of the dMyc-induced cell size increase together with a decrease in the number of cells per clone (Fig. 5E,F). Similarly, in polyploid salivary gland cells, dMyc overexpression on its own dramatically increased nuclear and overall cell size (Pierce et al., 2004) (Fig. 6A,B). However, when *vito*RNAi was co-expressed cell growth was considerably attenuated (Fig. 6A,B). This resulted from significant reductions in cytoplasmic (down by 59%, $P<1\times10^{-4}$) and nuclear (down by 70%, $P<1\times10^{-4}$) volumes when compared with dMyc overexpression (Fig. 6B). Therefore, genetically, *vito* lies downstream of dMyc in the control of cell growth and proliferation.

To identify the cellular function that *vito* performs during dMyc-stimulated cell growth, we examined whether Vito regulated nucleolar organisation when dMyc was overexpressed. As previously described (Grewal et al., 2005), dMyc overexpression in salivary gland cells led to an enlarged nucleus and nucleolus (Fig. 6A). When compared with the wild type, these nucleoli displayed slightly less compact packaging, with closely intermingled fibrillar and granular components. Crucially, when dMyc overexpression was induced together with *vito*RNAi, the nucleolus consistently displayed a segregated organisation, with a peripheral granular region surrounding an internal fibrillar area (Fig. 6A). This nucleolar structural arrangement resembles, in part, the structure of the *vito*RNAi-only nucleolus, although in the latter case the nucleolus shows a more decondensed granular region (compare Fig. 6A with Fig. 4H). Although these experiments involve partial knockdown and not null mutations, precluding definitive statements about epistasis, overall our findings suggest that *vito* lies downstream of *dMyc* in the control of *Drosophila* nucleolar structure.

DISCUSSION

Our data identify the *Nol12* homologue *vito* as an important regulator of dMyc function in the stimulation of nucleolar biogenesis and mass accumulation during *Drosophila* development. We show that dMyc controls *vito* mRNA levels to regulate nucleolar architecture and that *vito* is required for dMyc to reach its full potential as a potent cell growth inducer. Furthermore, the knockdown of *vito* expression also correlated with an increase in p53-independent, caspase-mediated apoptotic cell death, suggesting a potential novel link between structural and functional changes in the nucleolus and activation of the pro-apoptotic *rpr*/*grim*/*hid* complex.

During development, dMyc plays a crucial role in translating intracellular and extracellular cues to regulate the pace of cell growth and proliferation. One of the main mechanisms for dMyc-stimulated growth appears to be the transcriptional control of nucleolar ribosome biogenesis genes (Grewal et al., 2005; Hulf et al., 2005; Teleman et al., 2008; Demontis and Perrimon, 2009). Cells of the salivary glands are polyploid secretory cells with very active biosynthetic pathways. In these cells, increasing or reducing Vito levels results in changes in the nucleolar localisation patterns of the pre-rRNA methyltransferase Fibrillarin and in alterations in nucleolar structure. The fact that *vito* does not appear necessary for the expression of dMyc targets implicated in ribosomal biogenesis suggests that part of the control that dMyc exerts on the nucleolus is mediated independently of its regulation of *vito* expression. In addition, several results support the hypothesis that the Myc-Nol12 regulatory relationship is evolutionarily conserved. Genome-wide chromatin immunoprecipitation analysis has shown that c-MYC binds the *NOL12* promoter in both a human transformed B-cell line (Zeller et al., 2006) and in mouse stem cells (Kim et al., 2008). We have also identified non-canonical E-box motifs (CACATG) (Zeller et al., 2006) in the putative proximal promoter regions of both *vito* and human *NOL12* (data not shown).

In addition to its function in cell growth downstream of *dMyc*, *vito* plays a role in supporting the proliferation and survival of diploid cells. *dMyc* mutants are smaller than the wild type, and *dMyc* mutant cells grow poorly in the context of wild-type tissue (Johnston et al., 1999; Moreno and Basler, 2004; Benassayag et al., 2005; Wu and Johnston, 2010). Therefore, *vito* is a rate-limiting factor for tissue growth that links *dMyc* with nucleolar architecture. The mechanisms enacting this link might prove relevant for the regulation of Myc function in tumourigenesis (Meyer and Penn, 2008).

Acknowledgements

We thank Corinne Benassayag, Filipe Josué, Hermann Steller, Patrick DiMario, Robert Eisenman, the Bloomington *Drosophila* Stock Center, the Vienna *Drosophila* RNAi Center, and the Developmental Studies Hybridoma Bank for reagents; Inês Barbosa and Sofia Pinho for technical assistance; and Hélder Maiato and Vitor Barbosa for critical reading of the manuscript. This work was supported by grants PPCDT/BIA-BCM/56043/2004 (FCT, Portugal), and BFU2006-00349, BFU2009-07044 and Consolider 'From Genes to Shape' (MICINN, Spain) to F.C. J.M. was funded by FCT (SFRH/BD/33182/2007) and P.S.P. was funded by 'Programa Ciência' (FCT).

Competing interests statement

The authors declare no competing financial interests.

Supplementary material

Supplementary material for this article is available at
http://dev.biologists.org/lookup/suppl/doi:10.1242/dev.054411-/DC1

References

Ahmad, Y., Boisvert, F. M., Gregor, P., Cobley, A. and Lamond, A. I. (2008). NOPdb: Nucleolar Proteome Database – 2008 update. *Nucleic Acids Res.* **37**, D181-D184.

Arabi, A., Wu, S., Ridderstrale, K., Bierhoff, H., Shiue, C., Fatyol, K., Fahlen, S., Hydbring, P., Soderberg, O., Grummt, I. et al. (2005). c-Myc associates with ribosomal DNA and activates RNA polymerase I transcription. *Nat. Cell Biol.* **7**, 303-310.

Benassayag, C., Montero, L., Colombie, N., Gallant, P., Cribbs, D. and Morello, D. (2005). Human c-Myc isoforms differentially regulate cell growth and apoptosis in Drosophila melanogaster. *Mol. Cell. Biol.* **25**, 9897-9909.

Boisvert, F. M., van Koningsbruggen, S., Navascues, J. and Lamond, A. I. (2007). The multifunctional nucleolus. *Nat. Rev. Mol. Cell Biol.* **8**, 574-585.

Chen, H. K., Pai, C. Y., Huang, J. Y. and Yeh, N. H. (1999). Human Nopp140, which interacts with RNA polymerase I: implications for rRNA gene transcription and nucleolar structural organization. *Mol. Cell. Biol.* **19**, 8536-8546.

Chen, P., Nordstrom, W., Gish, B. and Abrams, J. M. (1996). grim, a novel cell death gene in Drosophila. *Genes Dev.* **10**, 1773-1782.

Cui, Z. and DiMario, P. J. (2007). RNAi knockdown of Nopp140 induces Minute-like phenotypes in Drosophila. *Mol. Biol. Cell* **18**, 2179-2191.

Demontis, F. and Perrimon, N. (2009). Integration of Insulin receptor/Foxo signaling and dMyc activity during muscle growth regulates body size in Drosophila. *Development* **136**, 983-993.

Edgar, B. A. and Orr-Weaver, T. L. (2001). Endoreplication cell cycles: more for less. *Cell* **105**, 297-306.

Emmott, E. and Hiscox, J. A. (2009). Nucleolar targeting: the hub of the matter. *EMBO Rep.* **10**, 231-238.

Grandori, C., Gomez-Roman, N., Felton-Edkins, Z. A., Ngouenet, C., Galloway, D. A., Eisenman, R. N. and White, R. J. (2005). c-Myc binds to human ribosomal DNA and stimulates transcription of rRNA genes by RNA polymerase I. *Nat. Cell Biol.* **7**, 311-318.

Grether, M. E., Abrams, J. M., Agapite, J., White, K. and Steller, H. (1995). The head involution defective gene of Drosophila melanogaster functions in programmed cell death. *Genes Dev.* **9**, 1694-1708.

Grewal, S. S., Li, L., Orian, A., Eisenman, R. N. and Edgar, B. A. (2005). Myc-dependent regulation of ribosomal RNA synthesis during Drosophila development. *Nat. Cell Biol.* **7**, 295-302.

Hulf, T., Bellosta, P., Furrer, M., Steiger, D., Svensson, D., Barbour, A. and Gallant, P. (2005). Whole-genome analysis reveals a strong positional bias of conserved dMyc-dependent E-boxes. *Mol. Cell. Biol.* **25**, 3401-3410.

Igaki, T. (2009). Correcting developmental errors by apoptosis: lessons from Drosophila JNK signaling. *Apoptosis* **14**, 1021-1028.

Johnston, L. A., Prober, D. A., Edgar, B. A., Eisenman, R. N. and Gallant, P. (1999). Drosophila myc regulates cellular growth during development. *Cell* **98**, 779-790.

Kim, J., Chu, J., Shen, X., Wang, J. and Orkin, S. H. (2008). An extended transcriptional network for pluripotency of embryonic stem cells. *Cell* **132**, 1049-1061.

Kuranaga, E., Kanuka, H., Igaki, T., Sawamoto, K., Ichijo, H., Okano, H. and Miura, M. (2002). Reaper-mediated inhibition of DIAP1-induced DTRAF1 degradation results in activation of JNK in Drosophila. *Nat. Cell Biol.* **4**, 705-710.

Li, Z., Lee, I., Moradi, E., Hung, N. J., Johnson, A. W. and Marcotte, E. M. (2009). Rational extension of the ribosome biogenesis pathway using network-guided genetics. *PLoS Biol.* **7**, e1000213.

Livak, K. J. and Schmittgen, T. D. (2001). Analysis of relative gene expression data using real-time quantitative PCR and the 2(-Delta Delta C(T)) method. *Methods* **25**, 402-408.

Martin-Blanco, E., Gampel, A., Ring, J., Virdee, K., Kirov, N., Tolkovsky, A. M. and Martinez-Arias, A. (1998). puckered encodes a phosphatase that mediates a feedback loop regulating JNK activity during dorsal closure in Drosophila. *Genes Dev.* **12**, 557-570.

McCain, J., Danzy, L., Hamdi, A., Dellafosse, O. and DiMario, P. (2006). Tracking nucleolar dynamics with GFP-Nopp140 during Drosophila oogenesis and embryogenesis. *Cell Tissue Res.* **323**, 105-115.

McEwen, D. G. and Peifer, M. (2005). Puckered, a Drosophila MAPK phosphatase, ensures cell viability by antagonizing JNK-induced apoptosis. *Development* **132**, 3935-3946.

Meyer, N. and Penn, L. Z. (2008). Reflecting on 25 years with MYC. *Nat. Rev. Cancer* **8**, 976-990.

Moreno, E. and Basler, K. (2004). dMyc transforms cells into super-competitors. *Cell* **117**, 117-129.

Nordstrom, W., Chen, P., Steller, H. and Abrams, J. M. (1996). Activation of the reaper gene during ectopic cell killing in Drosophila. *Dev. Biol.* **180**, 213-226.

Oeffinger, M., Zenklusen, D., Ferguson, A., Wei, K. E., El Hage, A., Tollervey, D., Chait, B. T., Singer, R. H. and Rout, M. P. (2009). Rrp17p is a eukaryotic exonuclease required for 5' end processing of Pre-60S ribosomal RNA. *Mol. Cell* **36**, 768-781.

Ollmann, M., Young, L. M., Di Como, C. J., Karim, F., Belvin, M., Robertson, S., Whittaker, K., Demsky, M., Fisher, W. W., Buchman, A. et al. (2000). Drosophila p53 is a structural and functional homolog of the tumor suppressor p53. *Cell* **101**, 91-101.

Orihara-Ono, M., Suzuki, E., Saito, M., Yoda, Y., Aigaki, T. and Hama, C. (2005). The slender lobes gene, identified by retarded mushroom body development, is required for proper nucleolar organization in Drosophila. *Dev. Biol.* **281**, 121-133.

Peng, W. T., Robinson, M. D., Mnaimneh, S., Krogan, N. J., Cagney, G., Morris, Q., Davierwala, A. P., Grigull, J., Yang, X., Zhang, W. et al. (2003). A panoramic view of yeast noncoding RNA processing. *Cell* **113**, 919-933.

Pfaffl, M. W., Horgan, G. W. and Dempfle, L. (2002). Relative expression software tool (REST) for group-wise comparison and statistical analysis of relative expression results in real-time PCR. *Nucleic Acids Res.* **30**, e36.

Pierce, S. B., Yost, C., Britton, J. S., Loo, L. W., Flynn, E. M., Edgar, B. A. and Eisenman, R. N. (2004). dMyc is required for larval growth and endoreplication in Drosophila. *Development* **131**, 2317-2327.

Pierce, S. B., Yost, C., Anderson, S. A., Flynn, E. M., Delrow, J. and Eisenman, R. N. (2008). Drosophila growth and development in the absence of dMyc and dMnt. *Dev. Biol.* **315**, 303-316.

Prieto, J. L. and McStay, B. (2007). Recruitment of factors linking transcription and processing of pre-rRNA to NOR chromatin is UBF-dependent and occurs independent of transcription in human cells. *Genes Dev.* **21**, 2041-2054.

Rubbi, C. P. and Milner, J. (2003). Disruption of the nucleolus mediates stabilization of p53 in response to DNA damage and other stresses. *EMBO J.* **22**, 6068-6077.

Suzuki, S., Fujiwara, T. and Kanno, M. (2007). Nucleolar protein Nop25 is involved in nucleolar architecture. *Biochem. Biophys. Res. Commun.* **358**, 1114-1119.

Teleman, A. A., Hietakangas, V., Sayadian, A. C. and Cohen, S. M. (2008). Nutritional control of protein biosynthetic capacity by insulin via Myc in Drosophila. *Cell Metab.* **7**, 21-32.

Wang, C., Query, C. C. and Meier, U. T. (2002). Immunopurified small nucleolar ribonucleoprotein particles pseudouridylate rRNA independently of their association with phosphorylated Nopp140. *Mol. Cell. Biol.* **22**, 8457-8466.

White, K., Grether, M. E., Abrams, J. M., Young, L., Farrell, K. and Steller, H. (1994). Genetic control of programmed cell death in Drosophila. *Science* **264**, 677-683.

Wu, D. C. and Johnston, L. A. (2010). Control of wing size and proportions by Drosophila myc. *Genetics* **184**, 199-211.

Yuan, X., Zhou, Y., Casanova, E., Chai, M., Kiss, E., Grone, H. J., Schutz, G. and Grummt, I. (2005). Genetic inactivation of the transcription factor TIF-IA leads to nucleolar disruption, cell cycle arrest, and p53-mediated apoptosis. *Mol. Cell* **19**, 77-87.

Zeller, K. I., Zhao, X., Lee, C. W., Chiu, K. P., Yao, F., Yustein, J. T., Ooi, H. S., Orlov, Y. L., Shahab, A., Yong, H. C. et al. (2006). Global mapping of c-Myc binding sites and target gene networks in human B cells. *Proc. Natl. Acad. Sci. USA* **103**, 17834-17839.